

RESEARCH ARTICLE

3D-QSAR, molecular docking studies, and binding mode prediction of thiolactomycin analogs as mtFabH inhibitors

Xiaoyun Lu, Yadong Chen, and Qidong You

Department of Medicinal Chemistry, China Pharmaceutical University, 24 Tongjiaxiang, Nanjing 210009, PR China

Abstract

Mycobacterium tuberculosis β -ketoacyl-acyl carrier protein synthase III (*mtFabH*) has been identified as a novel target for treating tuberculosis. The aim of this study was to understand the binding affinities of thiolactomycin (TLM) analogs for *mtFabH* based on 3D quantitative structure–activity relationship (3D-QSAR) analysis and molecular docking studies. The 3D-QSAR models produced statistically significant results (comparative molecular field analysis (CoMFA) r^2 cv=0.701, r^2 =0.988; comparative molecular similarity indices analysis (CoMSIA) r^2 cv=0.625, r^2 =0.969) with 40 TLM analogs. In particular, compounds possessing hydrogen bond acceptors attached to the end of side chains at the C5 position of TLM analogs may enhance their activity. The results of 3D-QSAR models were further compared with structure-based analysis using docking studies with the crystal structure of *mtFabH*. A plausible binding mode between TLM analogs and *mtFabH* is proposed.

Keywords: *mtFabH*; thiolactomycin analogs; 3D-QSAR; docking studies; binding mode

Introduction

Mycobacterium tuberculosis (MTB), one of the oldest and most pervasive human diseases in history, remains a global health problem. According to the World Health Organization (WHO), at least a third of the world's population is infected with MTB. The dangerous spread of tuberculosis (TB) is mainly due to its association with human immunodeficiency virus (HIV) infection, and the development of multi-drug-resistant strains of MTB (MDR-TB) and extensively drug-resistant strains of MTB (XDR-TB)¹. Furthermore, it has been more than 40 years since a new drug for TB was discovered. Thus, it is urgently desired to develop new anti-tubercular drugs, which are effective against TB.

As fatty acid biosynthesis in pathogenic microorganisms is essential for cell viability, the enzymes involved in the FAS pathway have recently attracted considerable interest, a genomics-driven target for antibacterial drug discovery. β -Ketoacyl-acyl carrier protein (ACP) synthase III (KAS III, FabH) is the bacterial condensing enzyme in gram-positive and gram-negative bacteria that initiates the FAB cycle by catalyzing the first condensation step between acetyl-coenzyme A (CoA) and malonyl-ACP. *Mycobacterium tuberculosis* β -ketoacyl-ACP synthase III (*mtFabH*) is a

homodimer, closely similar in topology and active-site structure to *Escherichia coli* FabH (*ecFabH*), with a CoA/malonyl-ACP-binding channel leading from the enzyme surface to the buried active-site cysteine residue. The pivotal role of *mtFabH*, combined with its unique structural features and ubiquitous occurrence in bacteria, has made it an excellent molecular target for the development of novel antimycobacterial agents.

Thiolactomycin (TLM, **1**) was the first example of a naturally occurring thiolactone to exhibit antibiotic activity (Figure 1)². It is a unique molecule that exhibits selective activity against only the dissociable type II fatty acid synthase (FAS-II). TLM inhibits MTB FAS-II by targeting β -ketoacyl-

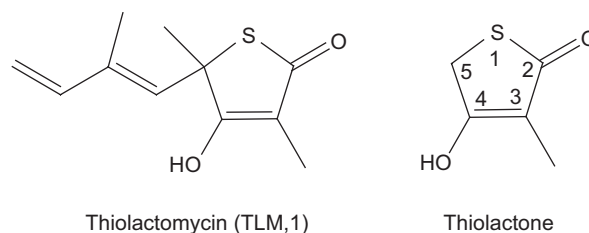


Figure 1. Structures of thiolactomycin (TLM, **1**) and thiolactone.

Address for Correspondence: Qidong You, Department of Medicinal Chemistry, China Pharmaceutical University, 24 Tongjiaxiang, Nanjing 210009, PR China. E-mail: youqidong@gmail.com

(Received 14 February 2009; revised 24 April 2009; accepted 28 April 2009)

ISSN 1475-6366 print/ISSN 1475-6374 online © 2010 Informa UK Ltd
DOI: 10.3109/14756360903049059

<http://www.informahealthcare.com/enz>

ACP synthase (*mtFabH* and *mtFabB*), *in vitro* and *in vivo*, leading to inhibition of cell wall mycolic acid biosynthesis and to cell death^{3,4}. Previous studies have shown that a number of TLM analogs exhibit moderate *mtFabH* inhibitory activity⁵⁻⁹, such as aromatic-acetylene and biphenyl analogs at the C5 position of TLM analogs. Further, the studies have revealed very little tolerance for substitutions at the C5 position of TLM in assays of condensing enzymes derived from MTB by Kim *et al.*⁸. Therefore, we have collected data on TLM analogs and carried out structural analysis using 3D-quantitative structure-activity relationship (QSAR) and docking methodologies. Furthermore, based on the 3D-QSAR models obtained and the docking results, we have gained insight into the molecular interactions between TLM analogs and *mtFabH* and propose a plausible binding mode for them.

We report herein the results of CoMFA (comparative molecular field analysis) and CoMSIA (comparative molecular similarity indices analysis) performed on a series of TLM analogs as *mtFabH* inhibitors. CoMFA¹⁰, the most popular 3D-QSAR method, has been chosen because of the renowned robustness of the model it produces. The CoMSIA¹¹ method differs in the way the molecular fields are calculated and by including additional molecular fields, such as lipophilic and hydrogen bond potential. Docking¹² programs predict the most likely conformation of how a ligand binds to a macromolecule. The aim was to analyze structural requirements of TLM analogs to understand the structural basis for their affinity to the catalytic center of the enzyme and to guide the design and synthesis of more potent inhibitors with predetermined affinities. Hitherto, no other computational study of TLM analogs targeting *mtFabH* can be found in the literature, and the 3D-QSAR models, docking studies, and predicted binding mode that we have obtained are reported for the first time.

Materials and methods

Data set

A series of TLM analogs (shown in Tables 1 and 2) reported as *mtFabH* inhibitors were considered in this study^{5,6,8,9}. The biological activities of the compounds were evaluated in the same laboratory. Biological activities measured as IC₅₀ were converted to pIC₅₀ ($-\log(\text{IC}_{50})$) for use in the 3D-QSAR study. To obtain a reliable and robust QSAR model, it is desirable to consider a data set that covers reasonable chemical diversity and biological activity. Selection of the training and test sets was done manually such that low, moderate, and high *mtFabH* inhibitory activity TLM analogs were present in roughly equal proportions in both sets. Thus, the test set was a true representative of the training set. The structures of the training and test set molecules are given in Tables 1 and 2, respectively.

Molecular modeling and alignment

All of the 3D structures of TLM analogs were built in molecular modeling software package Sybyl 6.9¹³. Partial atomic

charges were calculated by the Gasteiger-Huckel method, and energy minimizations were performed using the Tripos force field. Since the crystal structure of the *mtFabH*-TLM complex is not available, the least energy conformer was used as the bioactive conformation. The most potent aromatic-acetylene analog **3** was subjected to conformational search. The minimized conformer of compound **3** was taken as the template. The remaining molecules were aligned to it based on the basic core of thiolactone by the Align Database command available in Sybyl 6.9. The aligned molecules are shown in Figure 2. In addition to the 3D-QSAR analyses, docking simulations were performed using the X-ray crystallographic structure of *mtFabH* with long chain lauric acid substrate (Protein Data Bank (PDB) code: 1HZIP)¹⁴. The computer-simulated automated docking studies were performed using the widely distributed molecular docking software GOLD, based on the genetic algorithm (GA) method.

CoMFA

CoMFA is a widely used 3D-QSAR technique that relates the biological activity of a series of molecules with their steric and electrostatic fields. The region was created automatically, and the default grid spacing (2 Å) was employed. A sp³ hybridized carbon atom with a radius of 1.53 Å and a charge of +1.0 was used as a probe to calculate the steric and electrostatic energies between the probe and the molecules using the Tripos force field. Energy cutoff values of 30 kcal/mol were selected for both the electrostatic and steric fields. The experimental IC₅₀ (μM) values were converted into $-\log(\text{IC}_{50})$ values (Table 1) and used as the dependent column.

CoMSIA

Taking the same aligned molecules that were used for CoMFA, we performed the statistical evaluation for CoMSIA analysis, and some parameters were the same as for CoMFA. Five similarity fields, namely, steric, electrostatic, hydrophobic, hydrogen bond donor, and acceptor fields were evaluated at each lattice intersection of a regularly space grid of 2.0 Å. In optimizing CoMSIA performance, the most important parameter was how to combine the five fields in the CoMSIA model. In order to choose the optimal result, we

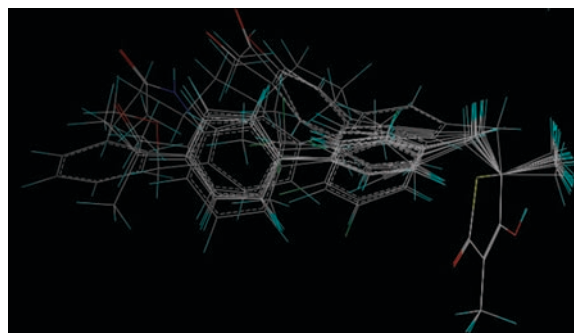
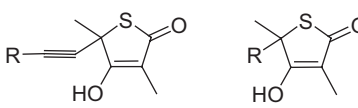
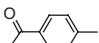
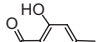
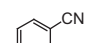
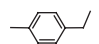
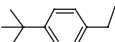
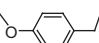
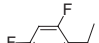
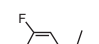
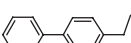
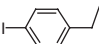
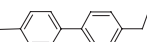
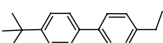
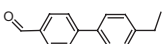
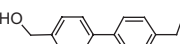
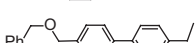

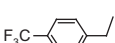


Figure 2. Alignment of training set molecules.

Table 1. Training set used for 3D-QSAR analysis.



Compounds **1-8** Compounds **9-40**

Compd	R	IC ₅₀ (μM)	pIC ₅₀	CoMFA		CoMSIA	
				PA ^a	Δ ^b	PA ^a	Δ ^b
1 (TLM)	—	74.9	4.13	4.093	0.037	4.136	-0.006
2	H—	100	4.00	4.001	-0.001	3.967	0.033
3		4	5.40	5.387	0.013	5.441	-0.041
4		7	5.15	5.160	-0.010	5.105	0.045
8		48	4.32	4.317	0.003	4.307	0.013
10		112	3.95	3.963	-0.013	3.988	-0.038
11		43	4.37	4.378	-0.008	4.244	0.126
12		155	3.81	3.792	0.018	3.809	0.001
15		246	3.61	3.624	-0.014	3.674	-0.064
16		263	3.58	3.598	-0.018	3.627	-0.047
17		51	4.29	4.245	0.045	4.257	0.033
19		153	3.82	3.817	0.003	3.734	0.086
20		52	4.28	4.324	-0.044	4.319	-0.039
21		25	4.60	4.619	-0.019	4.623	-0.023
22		29	4.54	4.545	-0.005	4.529	0.011
23		19	4.72	4.710	0.010	4.703	0.017
24		17	4.77	4.770	0.000	4.815	-0.045
25		119	3.92	3.893	0.027	3.933	-0.013
26	CH ₃ (CH ₂) ₁₁ CH ₂ —	80	4.10	4.124	-0.024	4.106	-0.006
27		100	4.00	4.000	0.000	4.041	-0.041

Note. The series was divided into a training set of 20 compounds (TLM included) and a test set of 20 compounds (Tables 1 and 2, respectively). The test set includes compounds representing all categories of activity of the training set, that is, inactive, active, and more active compounds comprising all structural features that are important for activity.

^aPredicted activity.

^bResidual of experimental and predicted activities.

systematically altered the combination of fields and chose those values which gave ideal non-cross-validation, standard errors of estimate, and *F*-values. Finally, to show five physicochemical properties, the model generated by combining the steric, electrostatic, hydrophobic, hydrogen bond acceptor, and donor fields was selected as the best CoMSIA model.

Partial least squares (PLS) analysis

Partial least squares (PLS)^{15,16} methodology was used for all 3D-QSAR analyses. The cross-validation^{17,18} analysis was performed using the leave-one-out (LOO) method, in which one compound is removed from the data set and its activity is predicted using the model derived from the rest of the data set. The cross-validated *r*² that resulted in the

Table 2. Test set used for 3D-QSAR analysis.

Compd	R	IC ₅₀ (μM)	pIC ₅₀	CoMFA		CoMSIA	
				PA ^a	Δ ^b	PA ^a	Δ ^b
5		74	4.13	4.160	-0.030	4.348	-0.218
6		34	4.47	4.162	0.308	4.544	-0.074
7		7	5.15	5.305	-0.155	5.100	0.050
9		250	3.60	4.103	-0.503	4.099	-0.499
13		500	3.30	3.173	0.127	3.092	0.208
14		52	4.28	4.236	0.044	4.067	-0.213
18		215	3.67	4.192	-0.522	4.065	-0.395
28		130	3.88	4.314	-0.434	4.103	-0.223
29		156	3.80	4.312	-0.512	4.106	-0.306
30		150	3.82	3.760	0.060	3.699	0.121
31		135	3.87	4.304	-0.434	4.070	-0.200
32		207	3.68	3.527	0.153	4.121	-0.441
33		105	3.98	4.450	0.470	4.094	-0.114
34		68	4.16	4.503	-0.343	4.114	0.046
35		200	3.69	3.434	0.256	4.121	-0.431
36		86	4.06	4.580	-0.520	4.123	-0.063
37		7	5.15	5.487	-0.337	5.599	-0.449
38		4	5.40	5.301	0.099	5.083	0.317
39		3	5.52	5.868	-0.348	5.382	0.138
40		283	3.55	3.178	0.372	4.079	-0.529

^aPredicted activity.^bResidual of experimental and predicted activities.

optimum number of components and the lowest standard error of prediction were considered for further analysis. To speed up the analysis and reduce noise, a minimum filter value σ of 2.00 kcal/mol was used. Final analysis was performed to calculate conventional r^2 using the optimum number of components obtained from the cross-validation analysis.

The predictive power of the 3D-QSAR models was determined from a set of 20 molecules that were excluded during model development. The optimization, alignment, and all other steps for these test set molecules were the same as those of the training set molecules, described

above, and their activities were predicted using the model produced by the training set. The predictive correlation (r^2_{pred}) based on the test set molecules was computed using:

$$r^2_{\text{pred}} = (\text{SD} - \text{PRESS}) / \text{SD}$$

where SD is defined as the sum of the squared deviations between the biological activities of the test set and mean activity of the training set molecules, and PRESS is the sum of the squared deviations between the predicted and actual activity values for each molecule in the test set.

Docking study

In order to investigate the appropriate binding orientations of TLM analogs interacting with the *mtFabH* crystal structure, a docking procedure was performed. The advanced molecular docking program GOLD¹⁹, version 3.1, which uses a powerful genetic algorithm (GA) method for conformational search and docking and is widely regarded as one of the best docking programs²⁰, was employed to generate an ensemble of docked conformations. Another advantage of using GOLD is that it applies some flexibility to the active site side chains¹⁹.

The original ligand, lauric acid, as well as water molecules in the target protein were removed from the coordinated set. Hydrogen atoms were added to the protein and Kollman all-atom charge was assigned. The genetic operators were 100 for the population size, 1.1 for the selection, 5 for the number of subpopulations, 100,000 for the maximum number of genetic applications, and 2 for the size of the niche used to increase population diversity. The weights were chosen so that cross-over mutations were applied with equal probability (95/95 for the values) and migration was applied 5% of the time. The ChemScore function encoded in GOLD was applied to predict the binding mode of *mtFabH* and 40 TLM analogs. This scoring function was described by Eldridge *et al.*²¹. The fitness score was taken as the negative of the sum of the component energy terms, so that larger fitness scores were better. The center of the bound lauric acid was defined as the binding site. Ten docking runs were performed per structure. All poses were output into a single *.sdf file.

To test whether the GOLD program was feasible for ligand binding to *mtFabH*, the lauric acid-*mtFabH* complex structure (PDB code: 1HZP) was initially chosen, and the docking structure of compound lauric acid was compared with its crystallographic structure. The resulting docked conformation of lauric acid and that of the crystallographic structure were very similar (root mean square deviation (RMSD): 0.67 Å). This result indicated that GOLD analysis may be suitable for identification of the binding mode of TLM analogs and *mtFabH*.

Results and discussion

Statistical analysis

CoMFA and CoMSIA models were derived from a training set of 20 structurally similar TLM analogs with IC₅₀ values ranging from 4 to 250 μM. The training set compounds were aligned on a minimum energy conformation of compound **3**, obtained by using the Random Search option given in Sybyl 6.9. The final predictions were obtained with the CoMFA standard model (r^2 cv=0.701, r^2 =0.988) and CoMSIA combined steric, electrostatic, hydrophobic, hydrogen bond donor, and hydrogen bond acceptor fields (r^2 cv=0.625, r^2 =0.969). The results of CoMFA and CoMSIA analysis are summarized in Table 3. The predictive correlation coefficient (r^2 pred) indicates a good statistical correlation and reasonable predictability of the CoMFA and CoMSIA models. Figure 3 shows the correlation between the actual values

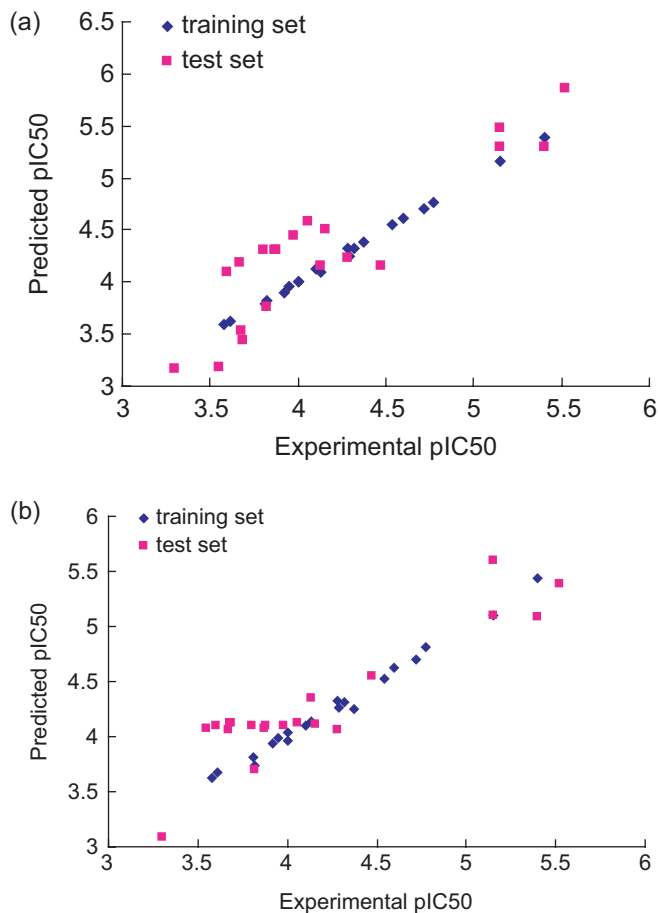


Figure 3. (a) Correlation between experimental pIC₅₀ and CoMFA predicted pIC₅₀ for training and test sets. (b) Correlation between experimental pIC₅₀ and CoMSIA predicted pIC₅₀ for training and test sets.

Table 3. Summary of 3D-QSAR analysis results obtained using CoMFA and CoMSIA.

Parameter	CoMFA	CoMSIA			
		S, E	S, E, H	S, E, D, A	All
r^2 cv	0.701	0.622	0.671	0.567	0.625
n	4	4	8	5	5
r^2	0.988	0.984	0.999	0.987	0.969
SEE	0.059	0.068	0.009	0.063	0.093
F -value	312.582	233.991	6646.700	219.655	167.576
Contribution					
Steric	0.557	0.363	0.250	0.274	0.163
Electrostatic	0.443	0.637	0.438	0.329	0.226
Donor				0.086	0.204
Acceptor				0.311	0.096
Hydrophobic			0.312		0.311
r^2 pred	0.818				0.833

Note. r^2 cv, cross-validated correlation coefficient; n , no. of components; r^2 , conventional correlation coefficient; SEE, standard error of estimate; F -value, F -test value; S, steric field; E, electrostatic field; H, hydrophobic field; D, hydrogen bond donor field; A, hydrogen bond acceptor field; r^2 pred, predicted correlation coefficient for test set of compounds.

and predicted values from the final CoMFA and CoMSIA models.

CoMFA model

To visualize the information contents of the derived 3D-QSAR models, CoMFA contour maps were generated. The CoMFA contour plots of steric and electrostatic interactions are shown in Figure 4. In Figure 4a, the green contour around the benzene ring of the proper side chain indicates that steric bulk is favored there. As a consequence, when substituted by phenyl, it shows greater activity. This can be seen with compound **3** in which incorporation of the phenyl group results in an increase of activity as compared to compound **2**. The large yellow contour near the acetylene indicates that steric bulk is disfavored. So, when acetylene is replaced by the bulky phenyl group, it is disfavored, with less activity. This is in agreement with the fact that the activities of compounds **2–8**, with the less bulky acetylene group, are higher than those of the bulky phenyl group compounds **13**, **18**, and **40**. Another two yellow contours at the end of the side chain are found to be critical for reducing activity; for example, in the disubstituted fluoride containing analogs **31** and **32**, only substitutions at the *para* position of the benzene ring enhance the activity.

In Figure 4b, the red contour near the carbonyl group of the side chain indicates that any negative charge is favored there. For example, compounds **3**, **4**, **7**, **37**, **38**, and **39** show excellent activities for *mtFabH*. As a consequence, when a positively charged group or no groups are at the *para* position of the phenyl, this causes significant loss of potency. This can be seen with compounds **8**, **10**, and **11**, etc., positively charged or no groups oriented in a red contour, which may miss important interactions in the active site. The blue contour close to the phenyl indicates a favorable region for positive charge.

CoMSIA model

Figure 5a depicts the steric and electrostatic contour maps of CoMSIA. The green contour around the benzene ring of the proper side chain indicates that steric bulk is favored there, whereas the yellow contour near the acetylene indicates a sterically disfavored region; the red contour near the carbonyl group of the side chain indicates that any negative

charge is favored there, whereas the blue contour close to the phenyl indicates a favorable region for positive charge. These contours are also seen in the CoMFA maps and demonstrate similar results. In addition, there is another steric unfavored yellow contour near the end of the side chain in CoMSIA maps.

The hydrophobic contour map of CoMSIA is presented in Figure 5b. The yellow contour indicates that any hydrophobic group substituent here is favored. This can be explained by the fact that when the *meta* benzyloxy group of compound **14** is substituted by the methoxy group, like compound **15**, it shows a 10-fold improvement in potency. The hydrophilic favored white contour around the end of the side chain implies that any hydrophilic substitution is favored there. This can be explained by the fact that substitution by the *para* methyl group of compound **20** is less potent than substitution by the hydroxymethyl group of compound **23**.

Figure 5c and d depicts the CoMSIA H-bond donor and H-bond acceptor contour maps, respectively. The small cyan contour beside the phenyl indicates that hydrogen-bond-donating substituents should be favored in these regions, whereas the purple contour indicates that hydrogen-bond-donating substituents are disfavored (Figure 5c). This can also be seen in the hydrogen-bond acceptor contour map (Figure 5d). The area highlighted in magenta represents the region where hydrogen-bond-acceptor substituents are favored. Therefore, placement of hydrogen-bond-acceptor functions directing to this magenta contour is correlated with an enhancement of binding affinity. These observations are supported by the active compounds **3**, **4**, **37**, **38**, and **39**.

Docking study

To explore the detailed binding mode of TLM analogs and *mtFabH*, the advanced molecular docking program GOLD 3.1 was used. Three-dimensional structural information on the target protein was taken from the PDB entry 1HZP, with a resolution of 2.1 Å. All of the TLM analogs were docked into the active site of *mtFabH* with similar conformations. We selected TLM, the template compound **3**, and the most potent biphenyl compound **39** with *mtFabH* to analyze the binding interactions (Figure 6). In the model of the TLM-*mtFabH* complex (Figure 6a), the isoprenoid branch of TLM extends to the slender hydrophobic pocket directing

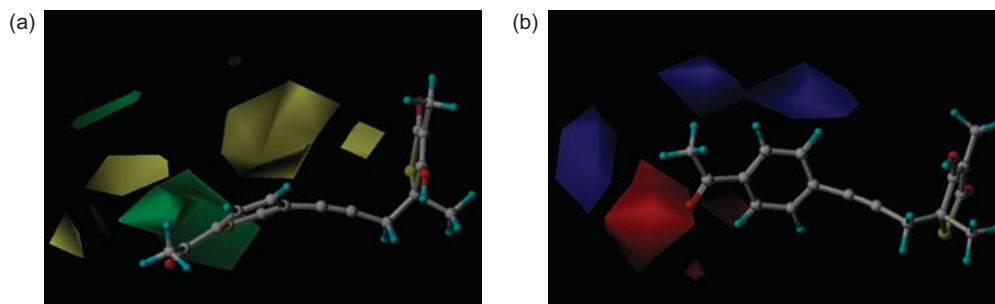


Figure 4. CoMFA contour maps. (a) Regions where increasing molecular volume increases bioactivity are in green, and regions where increasing molecular volume decreases activity are in yellow. (b) Regions where increasing positive charges increases activity are in blue, and regions where increasing negative charges increases activity are in red. Compound **3**, the template, is superimposed on both maps.

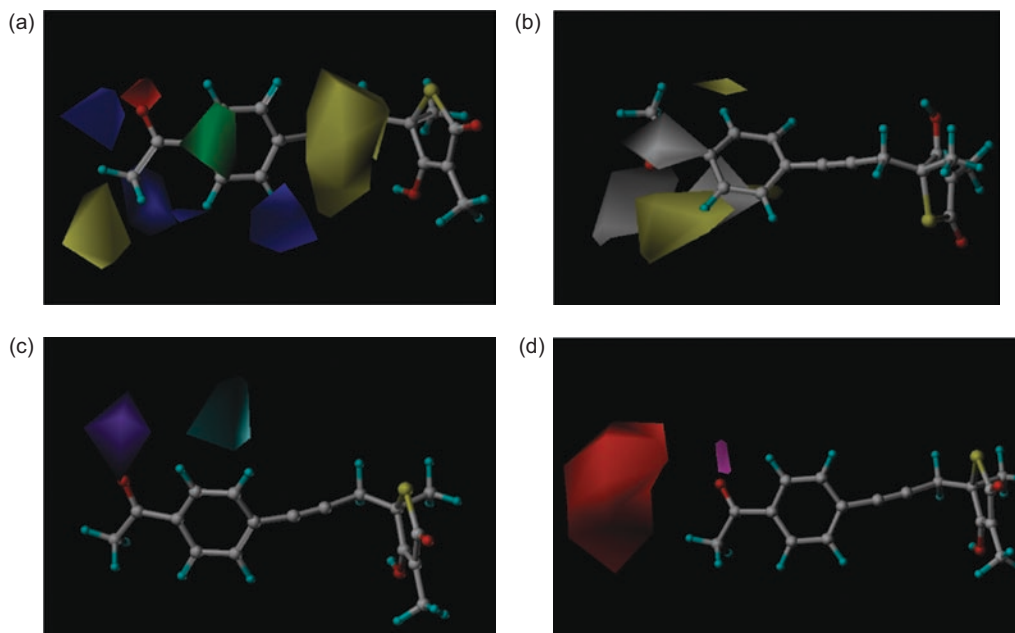


Figure 5. CoMSIA contour maps. (a) CoMSIA steric and electrostatic contour map. Green and yellow represent sterically favored and disfavored regions, respectively. Blue and red represent electrically favored and disfavored regions, respectively. (b) CoMSIA hydrophobic field contour map. Yellow regions indicate where hydrophobic groups increase activity and white regions indicate areas where hydrophilic groups increase activity. (c) CoMSIA H-bond donor contour map. Cyan contour indicates regions where hydrogen bond donor groups increase activity. Purple is disfavored. (d) CoMSIA H-bond acceptor contour map. Magenta contour indicates regions where hydrogen bond acceptor groups increase activity. Red is disfavored. Compound **3**, the template, is overlaid in each plot.

active site catalytic triad Cys112–His244–Asn274¹⁴, like the *mtFabH*–lauric acid binary complex, while the thiolactone moiety locates in the surface of the active site. The side chain at the C5 position of TLM possesses conjugate-double bonds to form hydrophobic and π stacking interactions within the small hydrophobic channel of *mtFabH*, while only one hydrogen bond is observed in the docked complex. The acetylene-based side chain at the C5 position of compound **3** fits into the small hydrophobic channel, with the hydrogen bonds between the carbonyl group and residues Asn274 and His244 and thiolactone moiety located in the surface of the active site with the hydrogen bond between the hydroxy group and residue Gly152 (Figure 6b). The biphenyl-based side chain at the C5 position of compound **39** also fits into the small hydrophobic channel, with the hydrogen bond between the carbonyl group and residues Asn274 and His244, and the thiolactone moiety located in the surface of the active site, with the hydrogen bond between the C4 hydroxy group and residue Gly152 (Figure 6c). Due to the same hydrogen bond between the carbonyl group and residues Asn274 and His244, compounds **3** and **39** exhibit good inhibitory activity against *mtFabH* with IC_{50} values 4 μ M and 3 μ M, respectively.

Compared to the binding modes of TLM with *ecFabB*²² (PDB code: 1FJ4) and with *mtFabB*²³ (PDB code: 2GP6), TLM binds with *mtFabH* at reverse orientation in our modeling. Modeling of TLM analog binding with *mtFabH* also elucidates that they fit the active site of *mtFabH*, unlike with *mtFabB*. This is in agreement with a previous study²⁴, which showed that FabB was sensitive to TLM while FabH was less sensitive. In the *ecFabB*–TLM binary complex, TLM O1 forms

strong hydrogen bond interactions with the two catalytic residues His298 and His333, and the C5 unsaturated alkyl side chain interaction with the small hydrophobic pocket is stabilized by π stacking interactions. In the model of the *mtFabB*–TLM complex²³, the isoprenoid branch of TLM also fits the small hydrophobic pocket composed of residues 270–280 and 405–406, while the thiolactone of TLM cannot form hydrogen bond interactions with the active site catalytic triad Cys170–His311–His346.

Despite the three proteins having similar catalytic triad active sites, the structural information indicates that the strong hydrogen bond interactions between the two active sites His–His and the O1 of TLM are important determinants of high affinity TLM binding. The *mtFabH* has a Cys112–His244–Asn274 catalytic triad, and is much less sensitive to TLM²². There may exist some differences at the surfaces surrounding the mouth of the channel, such as polar/charged amino acid and steric bulk in each active site²⁵. In the model of TLM–*mtFabH* (Figure 6a), the unsaturated side chain at the C5 position of TLM analogs extends to the slender hydrophobic pocket directing the Cys112–His244–Asn274 catalytic triad, like the *mtFabH*–lauric acid binary complex, while the thiolactone moiety locates in the surface of the active site. Comparing **3**–*mtFabH* and **39**–*mtFabH* with the TLM–*mtFabH* complex model, the results indicate that the end of the side chain at the C5 position of TLM analogs forming hydrogen bonds or a non-covalent bond with the active site Cys112–His244–Asn274 may increase the activity. In the surface of the catalytic triad, the C4 hydroxyl group of the thiolactone moiety forming a hydrogen bond may also enhance interactions with *mtFabH*. The common

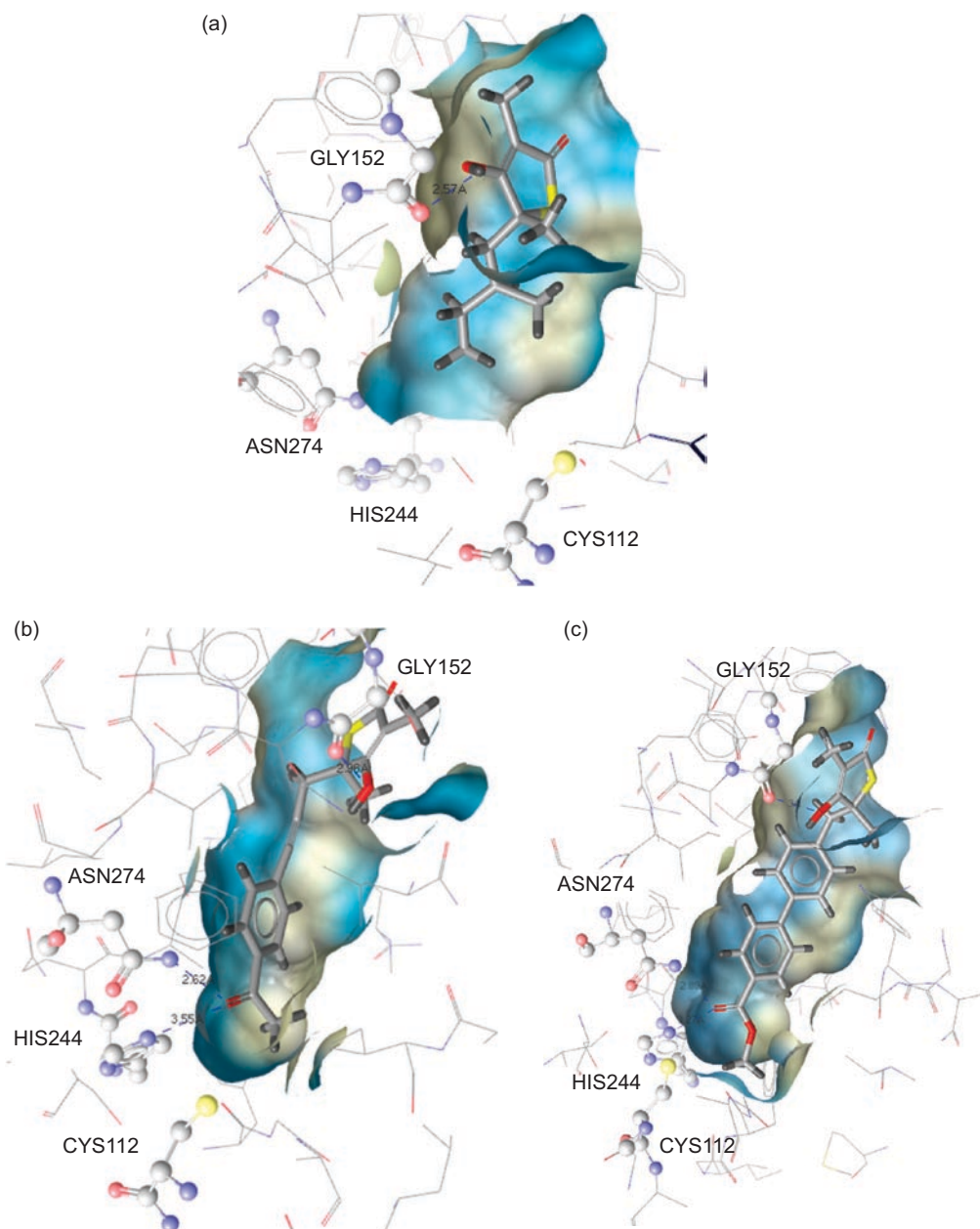


Figure 6. Modeling conformation of (a) thiolactomycin (TLM), (b) compound **3**, and (c) compound **39** in the binding site of *mtFabH* by the GOLD 3.1 program.

feature of the three complexes is the conjugate-structure side chains at the C5 position of TLM analogs embedding in the small hydrophobic channel of *mtFabH* with similar conformations (Figure 6).

Prediction of the binding mode

Based on the present 3D-QSAR and docking studies, 2D depiction of the hypothetical binding model of TLM analogs to *mtFabH* can be proposed (Figure 7) using LigandScout 2.0²⁶. Unsaturated side chains at the C5 position of TLM analogs extend to the slender hydrophobic pocket directing the active site catalytic triad Cys112–His244–Asn274 of *mtFabH*, while the common structure-thiolactone moiety locates in the surface of the catalytic triad. Hydrogen bonds can be observed between the carbonyl group and residues Asn274

and His244 and between the C4 hydroxy group of the thiolactone moiety and residue Gly152. Conjugate-structures at the C5 position also form hydrophobic and π stacking interactions with the active channel of the receptor. Due to the slender lauric acid binding channel, conjugate-structures that are less sterically hindered may enhance activity²⁷.

The models of 3D-QSAR elucidate the docking binding mode well. The hydrogen bond-accepting substitutions/negative charges (from 3D-QSAR results) attached to the end of side chains at the C5 position of TLM analogs play a vital role in the activity, because the TLM analogs substituted by a carbonyl group or carboxyl group (i.e. compounds **3**, **37–39**) drastically change the activity. This can be explained by the docking studies, showing that the hydrogen bond-accepting substitutions display hydrogen bonds

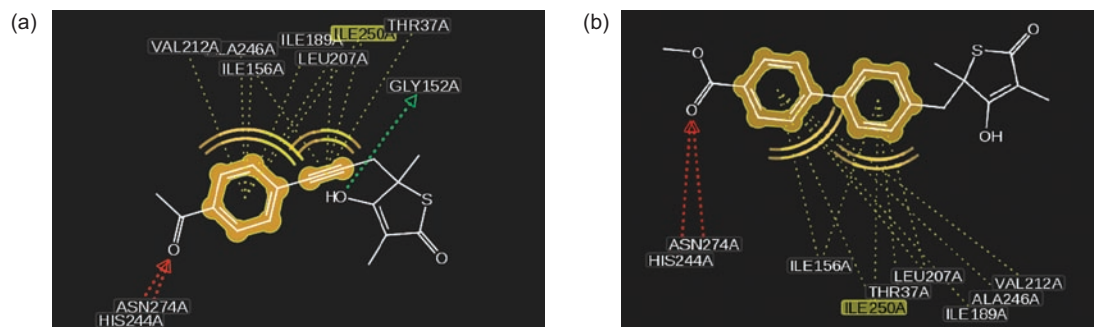


Figure 7. 2D depiction of the proposed binding mode of TLM analogs and *mtFabH* with hydrogen bond donors (green vectors), hydrogen bond acceptors (red vectors), and hydrophobic areas (yellow spheres): (a) compound **3** and (b) compound **39**.

with the active residues His244 and Asn274 (Figure 6). In the proposed binding mode, the hydrogen bond between the C4 hydroxy group of the thiolactone structure and residue Gly152 may also improve the activity. The studied binding mode is similar to how the carboxylic acid group of platencin interacts with Asn274 and His 244 of FabH²⁸.

Conclusion

In summary, as the crystallographic data for TLM bound with *mtFabH* is not available, computational studies have been performed on 40 TLM analogs using CoMFA, CoMSIA, and molecular docking studies. The predictions were obtained by the CoMFA model with r^2 cv of 0.701 and r^2 of 0.988 and CoMSIA model with r^2 cv of 0.625 and r^2 of 0.969, respectively. Docking approaches were applied to predict the binding mode between TLM analogs and *mtFabH*. The results show that unsaturated side chains at the C5 position of TLM analogs extend to the slender hydrophobic pocket directing the Cys112–His244–Asn274 catalytic triad of *mtFabH*, while the common structure-thiolactone moiety locates in the surface of the active site. In the binding mode, the end of the side chain at the C5 position of TLM analogs is proposed to interact with the Cys112–His244–Asn274 catalytic triad of *mtFabH* by hydrogen bond interactions and to be critical to the activity. Also, the conjugate-structures at the C5 position of TLM analogs that are less sterically hindered may improve the activity due to the slender lauric acid binding channel. In this study, the structure requirements for TLM analogs, as well as a plausible binding mode with *mtFabH*, are expected to be useful in the process of design and development of novel potent *mtFabH* inhibitors for treating TB.

Acknowledgements

This work was supported by Innovation Program for the Postgraduates in China Pharmaceutical University, P.R.China.

Declaration of interest

The authors report no conflicts of interest.

References

- World Health Organization. 2008 Tuberculosis Facts. Available at <http://www.who.int/tb>.
- Oishi H, Noto T, Sasaki H, Suzuki K, Hayashi T, Okazaki H, et al. Thiolactomycin, a new antibiotic. I. Taxonomy of the producing organism, fermentation and biological properties. *J Antibiot (Tokyo)* 1982;35:391–5.
- Schaeffer ML, Agnihotri G, Volker C, Kallender H, Brennan PJ, Lonsdale JT. Purification and biochemical characterization of the *Mycobacterium tuberculosis* beta-ketoacyl-acyl carrier protein synthases KasA and KasB. *J Biol Chem* 2001;276:47029–37.
- Kremer L, Dover LG, Carrere S, Nampoothiri KM, Lesjean S, Brown AK, et al. Mycolic acid biosynthesis and enzymic characterization of the beta-ketoacyl-ACP synthase A-condensing enzyme from *Mycobacterium tuberculosis*. *Biochem J* 2002;364:423–30.
- Senior SJ, Illarionov PA, Gurcha SS, Campbell IB, Schaeffer ML, Minnikin DE, et al. Biphenyl-based analogues of thiolactomycin, active against *Mycobacterium tuberculosis mtFabH* fatty acid condensing enzyme. *Bioorg Med Chem Lett* 2003;13:3685–8.
- Senior SJ, Illarionov PA, Gurcha SS, Campbell IB, Schaeffer ML, Minnikin DE, et al. Acetylene-based analogues of thiolactomycin, active against *Mycobacterium tuberculosis mtFabH* fatty acid condensing enzyme. *Bioorg Med Chem Lett* 2004;14:373–6.
- Kamal A, Shaik AA, Sinha R, Yadava JS, Arora SK. Antitubercular agents. Part 2: new thiolactomycin analogues active against *Mycobacterium tuberculosis*. *Bioorg Med Chem Lett* 2005;15:1927–9.
- Kim P, Zhang YM, Shenoy G, Nguyen QA, Boshoff HI, Manjunatha UH, et al. Structure-activity relationships at the 5-position of thiolactomycin: an intact (5R)-isoprene unit is required for activity against the condensing enzymes from *Mycobacterium tuberculosis* and *Escherichia coli*. *J Med Chem* 2006;49:159–71.
- Bhowruth V, Brown AK, Senior SJ, Snaith JS, Besra GS. Synthesis and biological evaluation of a C₅-biphenyl thiolactomycin library. *Bioorg Med Chem Lett* 2007;17:5643–6.
- Cramer RD, Patterson DE, Bunce JD. Comparative molecular field analysis (CoMFA). 1. Effect of shape on binding of steroids to carrier proteins. *J Am Chem Soc* 1988;110:5959–67.
- Klebe G, Abraham U, Mietzner T. Molecular similarity indices in a comparative analysis (CoMSIA) of drug molecules to correlate and predict their biological activity. *J Med Chem* 1994;37:4130–46.
- Leach AR, Shoichet BK, Peishoff CE. Prediction of protein-ligand interactions. Docking and scoring: successes and gaps. *J Med Chem* 2006;49:5851–5.
- Tripos. Sybyl molecular modeling software package; ver. 6.9. St. Louis, MO: Tripos Associates, Inc., 2003.
- Scarsdale JN, Kazanina G, He X, Reynolds KA, Wright HT. Crystal structure of the *Mycobacterium tuberculosis* beta-ketoacyl-acyl carrier protein synthase III. *J Biol Chem* 2001;276:20516–22.
- Wold S, Albano C, Dunn WJ III, Edlund U, Esbensen P, Geladi P, et al. In: Kowalski BR, ed. *Chemometrics—Mathematics and Statistics in Chemistry*. Dordrecht: Riedel Publishing Co., 1984: 17–95.
- Stahle L, Wold S. Partial least squares analysis with cross-validation for the two-class problem: a Monte Carlo study. *J Chemom* 1987;1:185–96.
- Cramer RD, Patterson DE, Bunce JD. Crossvalidation, bootstrapping, and partial least squares compared with multiple regression in conventional QSAR studies. *Quant Struct Act Relat* 1988;7:18–25.

18. Podlogar BL, Ferguson DM. QSAR and CoMFA: a perspective on the practical application to drug discovery. *Drug Des Discov* 2000;17:4-12.
19. Jones G, Willett P, Glen RC, Leach AR, Taylor R. Development and validation of a genetic algorithm for flexible docking. *J Mol Biol* 1997;267:727-48.
20. Kontoyianni M, McClellan LM, Sokol GS. Evaluation of docking performance: comparative data on docking algorithms. *J Med Chem* 2004;47:558-65.
21. Eldridge MD, Murray CW, Auton TR, Paolini GV, Mee RP. Empirical scoring functions: I. The development of a fast empirical scoring function to estimate the binding affinity of ligands in receptor complexes. *J Comput Aided Mol Des* 1997;11:425-45.
22. Price AC, Choi KH, Heath RJ, Li Z, White SW, Rock CO. Inhibition of beta-ketoacyl-acyl carrier protein synthases by thiolactomycin and cerulenin. Structure and mechanism. *J Biol Chem* 2001;276:6551-9.
23. Sridharan S, Wang L, Brown AK, Dover LG, Kremer L, Besra GS, et al. X-ray crystal structure of *Mycobacterium tuberculosis* beta-ketoacyl acyl carrier protein synthase II (mtKasB). *J Mol Biol* 2007;366:469-80.
24. Heath RJ, White SW, Rock CO. Lipid biosynthesis as a target for antibacterial agents. *Prog Lipid Res* 2001;40:467-97.
25. Alhamadsheh MM, Waters NC, Huddler DP, Kreishman-Deitrick M, Florova G, Reynolds KA. Synthesis and biological evaluation of thiazolidine-2-one 1,1-dioxide as inhibitors of *Escherichia coli* beta-ketoacyl-ACP-synthase III (FabH). *Bioorg Med Chem Lett* 2007;17:879-83.
26. Inte:Ligand. LigandScout ver. 2.0. Available at www.inteligand.com.
27. Castillo YP, Perez MA. Bacterial beta-ketoacyl-acyl carrier protein synthase III (FabH): an attractive target for the design of new broad-spectrum antimicrobial agents. *Mini Rev Med Chem* 2008;8:36-45.
28. Jayasuriya H, Herath KB, Zhang C, Zink DL, Basilio A, Genilloud O, et al. Isolation and structure of platencin: a FabH and FabF dual inhibitor with potent broad-spectrum antibiotic activity. *Angew Chem Int Ed Engl* 2007;46:4684-8.

Copyright of Journal of Enzyme Inhibition & Medicinal Chemistry is the property of Taylor & Francis Ltd and its content may not be copied or emailed to multiple sites or posted to a listserv without the copyright holder's express written permission. However, users may print, download, or email articles for individual use.